A four-component proxy model for total solar irradiance calibrated during solar cycles 21-23

C. Fröhlich

Physikalisch-Meteorologisches Observatorium Davos, World Radiation Center,
CH-7260 Davos Dorf, Switzerland, (E-mail: cfrohlich@pmodwrc.ch)

Abstract. The last solar activity minimum during 2008/09 was unusually long and with extended periods without sunspots. During this period the total solar irradiance (TSI) was much lower than during the previous minima and no solar activity proxies show similarly low values. Proxy models for TSI use a measure for the darkening of sunspots, the so-called photometric sunspot index (PSI) and for the brightening of faculae and network a chromospheric index. Because none of these can explain the low TSI, a further component is needed, which describes the trend between minima due to a still controversially discussed mechanism. A new algorithm for the calculation of PSI is described which uses individual factors for the different observing stations and a better representation of the size-dependent contrast of spots. The proxy model based on the new PSI, the long- and short-term Mg II index and a trend based on the minima values of the open field explains almost 85 % of the variance of TSI over the last three solar cycles. Moreover, it confirms the factor of ≈ 4 between the observed trend of TSI and those of the chromospheric and other solar activity indices.
Key words: total solar irradiance – solar activity – sunspots – faculae

1. Introduction

An unusually low TSI during the recent minimum was suggested by the observations as early as 2005 (*e.g.*, Fröhlich, 2006; Tapping *et al.*, 2007) from observations during the descending part of cycle 23. In late 2008/09 - during the minimum - TSI was more than 25 % lower, relative to its cycle amplitude, than during the previous minimum in 1996 (Fröhlich, 2009a). In contrast solar activity proxies like the sunspot number, the 10.7 cm radio flux or the chromospheric indices Ca II K and Mg II show only a decrease of the order of 4-6 % relative to their amplitudes; thus they show a decrease about four times smaller than TSI. Fröhlich (2009a) has found a strong correlation of TSI and the open magnetic field at 1 AU, $B_{\rm R}$, at solar activity minima which can be used to determine TSI when ever $B_{\rm R}$ is known. Proxy models for TSI based on the photometric sunspot index (PSI) for the sunspot darkening and, *e.g.*, the Mg II index for the facular and network enhancement of the irradiance explain very well the intra-cycle variation (see, *e.g.*, Fröhlich & Lean (2004) and references therein), but

the chromospheric indices are obviously unable to explain the strong downward trend of TSI during the last cycle. A pragmatic approach is to add a further component to the proxy model for the long-term variation, which is approximated by a linear trend between minima at which values of B_R are used as suggested by the correlation. In order to check the validity of this approach the proxy model itself has been improved, especially the determination of PSI which is now based on a new algorithm. Section 2 describes the data base for TSI and the activity indices, and the correlation with the open magnetic field at 1 AU. In Section 3 the proxy model is developed with a detailed description of the new algorithm for PSI and the discussion of the results is presented in Section 4 and the conclusions in Section 5.

2. Data basis

The basis for the TSI time series is the so-called PMOD composite which is a reliable description of solar variability during the last three cycles (see, *e.g.*, Fröhlich, 2006, 2009a; Lockwood & Fröhlich, 2008, and references therein) as shown in Fig. 1. The uncertainty of the PMOD composite during the last cycle has been discussed extensively in Fröhlich (2009a), together with a discussion of the differences to TIM/SORCE and ACRIM II/III. There are obvious changes on the solar rotation timescale (27-day) as, *e.g.*, during the passage of active regions with dips due to sunspots and rises due to faculae. Moreover, there is also a modulation with the 11-year period with changing characteristics from cycle to cycle. During the most recent cycle the number of sunspots was less than during the two cycles before (see Fig. 2a) and there were periods during high activity with essentially no spots, but faculae which made the TSI amplitude during this cycle of the same order as during the ones before. As in Fröhlich (2009a) the amplitude is defined as an equivalent of a sine square (twice the average between the minima of the considered quantity). For the last three cycles the amplitudes are with the above definition 0.9497, 0.9032, and 0.9671 Wm^{-2} and corrected for the trend between the minima during each cycle 0.9244, 0.8489, and 0.8507 Wm^{-2}, respectively. Moreover, an objective definition for the 'time of minimum' is needed and the first appearance of an important sunspot group of the new cycle is used (at high latitude and of opposite polarity). With this definition the dates of the last four minima are 10 October 1976, 19 September 1986, 21 August 1996, and 29 November 2008 (same as in Fröhlich, 2009a). It is interesting to note that the so defined minima do not necessarily coincide with the minima of the value of a given parameter as shown in Figs. 2 and 3.

Solar activity is driven by the magnetic fields produced periodically by a dynamo at the base of the convection zone (for a review see, *e.g.*, Charbonneau (2005) and references therein) and magnetic fields threading the visible solar surface, the photosphere produce features like sunspots, faculae, network and ephemeral regions. Fig. 2 shows time series of typical measures of solar activity
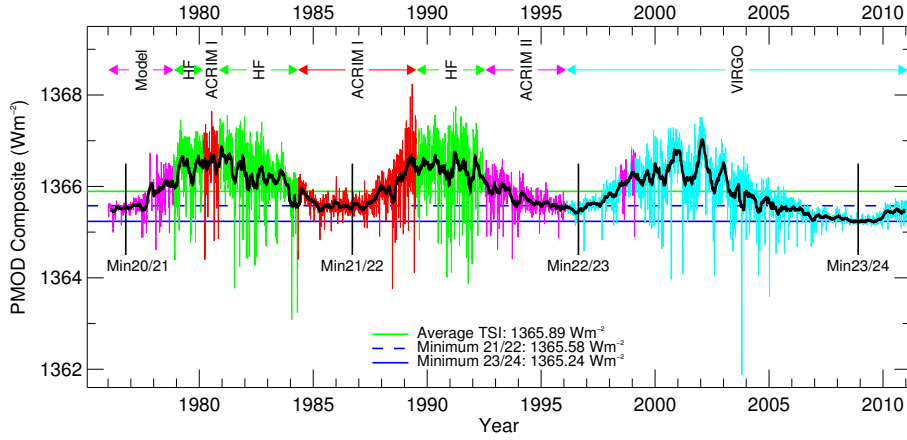
Figure 1. Daily TSI of the PMOD composite (updated until end of January 2011, Version 41_62_1102) and extrapolated with a proxy model back to 1976. The amplitudes of the three cycles decrease first and then increase again. The two horizontal lines indicate the value of the minima in 1986 and 2008, respectively. Note the low value of the 2008/9 minimum, which is $0.22\,\mathrm{Wm^{-2}}$ lower than the previous one, or $25\,\%$ in terms of an average cycle amplitude.

for solar cycles 20–23. The sunspot number (SSN, Fig. 2a) is certainly the most widely used index mainly because it is available since the 17th century, but also because its cycle amplitude represents a measure for the varying amount of bipolar regions reaching the surface and hence the strength of solar activity during a cycle. The next parameter is the solar radio flux at $10.7\,\mathrm{cm}$ (F 10.7, Fig. 2b) which is an absolute physical measurement available since 1947 (solar flux units $\equiv 10^{-22}\,\mathrm{Wm^{-2}\,Hz^{-1}}$) and is widely used as a surrogate for the UV and EUV radiation. A similar behavior show the Ca II K and Mg II indices (Figs. 2c and 2d) which represent changes of the chromosphere due to surface magnetic fields. None of these quantities show an important decrease during the recent minimum and the observed trends between minima, summarized in Tab. 1. The average for SSN, F 10.7, Ca II K and Mg II shows no significant changes over cycles 21 and 22, whereas the average change for cycle 23 is $-6.5 \pm 3.4\,\%$, which is 4.2 times smaller than the TSI change. The only parameter that does exhibit inter-cycle changes during the minima similar to TSI is the open magnetic field, B_R, as observed at 1 AU by satellites since the sixties (see Fig. 3 and Tab. 1). B_R used here is determined by taking the absolute value of the daily mean of B_X from the OMNI2 data set (available from `ftp://nssdcftp.gsfc.nasa.gov/spacecraft_data/omni/omni_m_daily.dat`). B_R at minima is mainly determined by the polar field of the Sun and is a good measure of the strength of solar activity, because this field is left over from the past cycle and provides
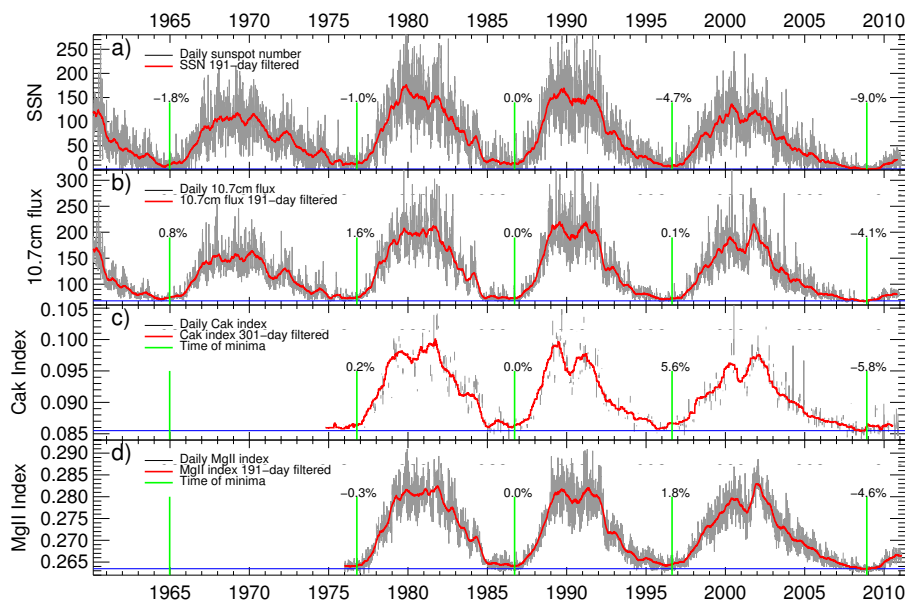
Figure 2. Daily values of the time series of a) SSN, b) F 10.7, c) Ca II K and d) Mg II indices. The values indicated at solar minima (above the vertical lines) are the percent changes relative to the amplitude of cycle 22 and normalized to the value between cycles 21 and 22 indicated by the horizontal blue line. In contrast to TSI of Fig. 1, none of these records show the large decrease during the present minimum.

the starting value for the next solar cycle. This correlation does not mean a direct physical link between the quantities; rather it confirms the suggested longer-time-scale dependence of TSI on the strength of the solar cycle. Such a relationship was first suggested by Eddy (1976) by showing that the Maunder Minimum (MM) in the 17th century may be an example of low solar activity and possibly low TSI, resulting in the "Little Ice Age" in Europe. The correlation of TSI with B_R can be used as a further component of a proxy model. Obviously, one could also discard the trend of TSI with the argument that it is only a 1.5-σ result as explained in Fröhlich (2009a). However, this uncertainty estimate is already conservative and from the experience with the development of the PMOD composite I am quite confident that the observed change is real (see also next Section).

3. Proxy model of total solar irradiance

Proxy models of TSI are based on daily indices representing the darkening of sunspots and the brightening by faculae and small magnetic elements. A 3-
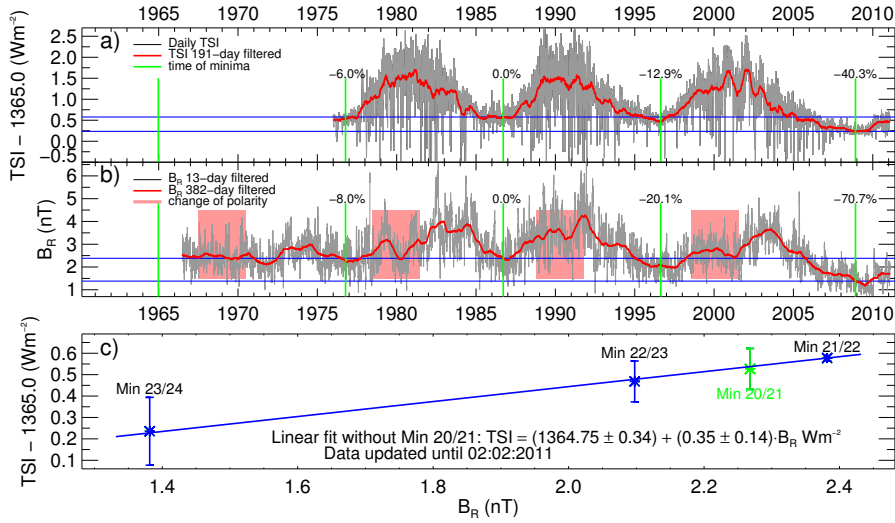
Figure 3. Comparison of TSI and the open solar magnetic field. a) daily values of TSI (as Fig. 1) and b) daily values of the open magnetic field B_R at 1 AU. The correlation between the minimum values of TSI and of B_R (blue points and the blue line) is shown on c). The green point is the extrapolated value not used in the regression. The error bars are from a detailed analysis as described in Fröhlich (2009a) and the errors of regression coefficients include these uncertainties, and hence are quite large (updated from Fig. 4 of Fröhlich (2009a)).

component model uses PSI for the influence of sunspots, ΔS_S, and two different indices for the brightening of faculae (a short-term variation at solar rotation timescales) and network (longer-term variation at timescales of many solar rotations), ΔS_F and ΔS_N (for a review see, *e.g.*, Fröhlich & Lean (2004) and references therein).

The need for a fourth component has been already shown by Fröhlich (2009b) and Steinhilber (2010). In a recent paper, however, Krivova *et al.* (2011) claim that there is no need for such a component because the observed trend in TSI is probably an instrumental artefact. The main reason for their claim is that the SATIRE model is unable to reproduce the difference between the minima in 1996 and 2008 observed in TSI. Although they adjust the free parameter of the SATIRE model to the TSI record over the full period of cycle 23, the fit is heavily weighted by the long descending phase of that cycle. The same result is found by Ball *et al.* (2011) using only the period of the SORCE observations starting in 2003 for the calibration of the SATIRE model. This makes the agreement best during the descending part of cycle 23 and produces an obviously large difference in 1996. In contrast, earlier results with the same SATIRE model by Wenzler

et al. (2006, 2009) and Krivova *et al.* (2003) show good agreement during the ascending phase of cycle 23 and the time back to 1978. Steinhilber (2010) based his SATIRE model on synoptic maps instead of individual magnetograms and calibrated it also during the ascending phase of the cycle and the results confirm the findings of Krivova *et al.* (2003) and as this analysis covers the full cycle a substantial discrepancy during the minimum 2008/09 is found. So, the reasoning for a fourth component for the 3-component proxy model is based on the same ground as the rejection of it by Krivova *et al.* (2011), namely the inability of both the SATIRE and the proxy model to show an important difference between the recent minima. Moreover, the TSI difference between 1996 and 2008 is also confirmed by the combined ACRIM II and III measurements (for details see on-line annex of Fröhlich, 2009a and Fröhlich, 2006). As long as no serious flaws in the VIRGO radiometry can be identified, one should accept the low value of TSI during the recent minimum.

So, we can now use the TSI–B_R correlation at minima – linearly interpolated between them – to represent the trend ΔS_T. The solar cycle is modulated by magnetic features with smaller sizes than faculae and distributed all over the sun as network. The small bipolar fields from "Ephemeral Regions" (see, *e.g.*, Harvey, 2000; Hagenaar *et al.*, 2008) are also included in this part. So, the 4-component proxy model of TSI can be constructed as

$$S(t) = S_Q + \sum \Delta S = S_Q + a_F P_F(t) + a_N P_N(t) + a_S P_S(t) + a_T P_T(t), \quad (1)$$

with the value of the quiet Sun, S_Q, and $a_{F,N,S,T}$ the four coefficients for the influence of faculae, network, sunspots and the trend. S_Q and $a_{F,N,S,T}$ are determined by a multi-linear regression between daily values of TSI and those of $P_{F,N,S,T}$ as shown in Section 4. Because faculae and sunspots are both occurring together in active regions, the coefficients $a_{F,S}$ may not really represent the part of their contribution due to mutual compensation.

3.1. Sunspot darkening

Sunspot darkening, the fractional change in TSI caused by sunspots, is calculated explicitly as

$$p_S = \frac{P_S}{S_Q} = \sum_i \frac{\Delta S_i}{S_Q} = \sum_i \mu_i A_i \alpha \frac{R(\mu_i)}{\int_0^1 R(\mu)\mu d\mu} \quad (2)$$

where ΔS_i is the reduction of irradiance relative to the quiet Sun, S_Q for a sunspot i with the area A_i (in fractions of the solar hemisphere, *e.g.*, in μhem which changes to ppm for PSI), at location μ_i in heliocentric coordinates and with the bolometric contrast α. $R(\mu)$ is the center-to-limb variation function which is assumed to be the same for the quiet photosphere and the spot, the summation is over all spots on the solar disk at a specific day. A new algorithm was developed in early 2010 and the results have been already used in, (*e.g.*,

Table 1. Cycle amplitudes and relative changes of minima in percent of the amplitude during cycle 22. The amplitudes are equivalent sine-squared with the trend during each cycle removed. The units are: TSI $(\mathrm{Wm^{-2}})$, the open field at $1\,\mathrm{AU}$ B_R (nT), SSN (number), F 10.7 (sfu $\equiv 10^{-22}\,\mathrm{Wm^{-2}\,Hz^{-1}}$), Ca II K and Mg II indices (core-to-wing ratio).

Parameter	Cycle 21	Cycle 22	Cycle 23	Average	StdDev
		corrected cycle amplitude			
TSI	0.9244	0.8489	0.8507	0.8747	0.0431
B_R	1.300	1.415	1.148	1.288	0.134
SSN	139.8	132.9	98.1	123.6	22.4
F 10.7	126.5	121.3	96.9	114.9	15.8
Ca II K	0.0129	0.0095	0.0081	0.0102	0.0025
Mg II	0.0175	0.0151	0.0137	0.0154	0.0019
		change of minima over each cycle in percent			
TSI	6.0	−12.9	**−27.4**	−11.4	16.8
B_R	8.1	−20.1	**−50.6**	−20.9	29.3
SSN	1.0	−4.7	−4.3	−2.7	3.2
F 10.7	1.6	0.1	−4.0	−0.8	2.9
Ca II K	−0.2	5.6	−11.4	−2.0	8.7
Mg II	0.3	1.8	−6.4	−1.4	4.4
Average SSN$\cdots$Mg II	0.7 ± 0.8	0.7 ± 4.3	$−6.5 \pm 3.4$		

Fröhlich, 2011a, 2011b) without a detailed description, which is now presented here.

The basic time-dependent information about sunspot areas and locations are from white light images made from 1874 to 1976 by the Royal Greenwich Observatory (RGO) and since 1969 from sunspot drawings by the Solar Environment Laboratory (SEL) of the National Oceanographic and Atmospheric Administration (NOAA) together with those of stations of the United States Air Force (USAF). For data up to December 1981 their origin is termed as USAF/NOAA, afterwards the data are from an extended network of observatories, now called Solar Observation Optical Network (SOON). These data, and those from other stations such as Rome, Catania, Debrecen, USSR, Taipei, are now available from the National Geophysical Data Center (NGDC) operated by NOAA at Boulder, Colorado from `ftp://ftp.ngdc.noaa.gov/STP/SOLAR_DATA/SUNSPOT_REGIONS/`. The RGO data have been digitized from the Annals by Hoyt & Eddy (1982) and after the termination of the RGO operation at the end of 1976 measurements of the USAF/NOAA network were added up to 1981 (available from NGDC directory 'Greenwich' for the years 1874-1981). The early USAF/NOAA data were published since 1969 in the Solar Geophysical Data (SGD) monthly reports (available in electronic form from NGDC directory 'SGD_Table'). However, comparisons in the early 90ties (*e.g.*, Pap, 1993) have

shown that these data are not identical to those published in the reports, having many missing and unreliable data - at least during the period 1978-1982 investigated. Thus, the data from Hoyt & Eddy (1982) are used here, which seem to be the original USAF/NOAA ones. Earlier, these data were directly available as 'USAF_MWL.YY' annual files with the station identification 'GREE' and have been used extensively; some time ago they were removed from NGDC. After December 1981 the data from SOON are used (available from NGDC directory 'USAF_MWL'). In this analysis two more stations have been added to this data set, namely the observations from Tashkent and Ussurijsk (formerly Voroshilov) since 1998 (available from NGDC directories 'Tashkent' and 'Voroshilov'). It should also be noted that with the start of the SOON data set in December 1981 a major change in the determination of the area has been made. Before the areas were determined by overlaying a grid (1 mm or ≈ 10 arcsec spacing) and by counting the number of cells covered and after by a new overlay providing circles and ellipses of different size (a description is at `/STP/SOLAR_DATA/SUNSPOT_REGIONS_old/USAF_MWL/SunspotAreaMetadata.txt` and the new overlay as `SpotAreaCorrectionOverlay.jpg`). The use of this new overlay may also be the reason why the areas are rounded to 10, which adds some uncertainty mainly during solar minima (see also Balmaceda *et al.*, 2009).

In order to produce a homogeneous data set since 1874 Balmaceda *et al.* (2009) compared the RGO sunspot areas until 1976 with those from SOON after 1982 via USSR data from 1968–1991 (available from NGDC directory 'USSR_Solar_Data'). They report a difference of about 40 % with the RGO areas being higher than the SOON ones, confirming a value which was already published by Hathaway *et al.* (2002) (see also `http://solarscience.msfc.nasa.gov/greenwch.shtml`). As the early USAF/NOAA sunspot data (1972-1981) together with the SOON data were used extensively for calculating PSI (*e.g.*, Hudson & Willson, 1981; Hoyt *et al.*, 1983; Fröhlich *et al.*, 1994; Fröhlich & Lean, 2004) it seemed adequate to see whether this 40 % difference is also applicable for the USAF/NOAA data during 1977–1981.

Furthermore, I used this opportunity to update my old FORTRAN program to calculate PSI which was developed to implement the algorithms described in Fröhlich *et al.* (1994). Before PSI can be calculated, daily values of the average area and position for each spot group are needed. This was originally done by calculating daily means for each observation and by averaging the results from different stations. As the time series of the hemispheric area of a region shows the evolution of the spot group, a smooth function in time to all observations of the area of the same region would certainly be a more appropriate method to determine a reliable average. The new algorithm uses a polynomial with a degree increasing from zero to three with an increasing number of observations and days within the region. This procedure is applied to the observations of many regions over many years, *e.g.*, the SOON data from 1981 until 2008 and allows to determine also a statistics of possible differences between the contributing stations. If the data from one station deviates too much from the fit it is removed

Table 2. List of the SOON stations, with their abbreviation ID indicated in the data files, the location, time difference Δt in hh:mm and the correction factor C as a ratio of the observed to the average. The average of the correction factor for the SOON stations is 0.983 ± 0.038 which is within the 1-σ uncertainty equal to 1.000. From 1975-1979 Boulder, Ramey and Manila were the only stations contributing to these early USAF/NOAA data, Palehua joined during 1979, Holloman and Learmont in early 1981. Ussurijsk was named in 1935 Voroshilov, which was the official name until 1957.

Name	ID	Lat	Long	Δt	C
Athens, Greece	ATHN	37.99	23.75	1:35	0.888
Boulder, CO USA	BOUL	40.0	−105.3	−7:01	0.881
Holloman, NM, USA	HOLL	33.0	−106.0	−7:04	1.015
Learmont, Australia	LEAR	−22.22	114.1	7:36	0.983
Manila, Philipines	MANI	14.39	120.59	8:02	1.238
Palehua, HI, USA	PALE	21.24	−158.06	−10:32	0.961
Ramey, Puerto Rico	RAMY	18.0	−67.0	−4:28	1.030
San Vito, Italy	SVTO	40.4	17.43	1:10	1.021
Culgora, Australia	CULG	−30.3	149.6	9:58	0.834
Tashkent, Uzbekistan	TACH	41.33	69.30	4:37	1.087
Ussurijsk, Russian Federation	VORO	43.78	132.03	8:48	1.394

as outlier, but its deviation from the fit without outlier is still retained in the station statistic. So, during a next run of the analysis which uses the correction factors determined from the statistics of the previous run, this station may now be included with a corresponding correction factor. After about three runs the correction factors no longer change and can be saved as definitive results. The list of stations is presented in Tab. 2, together with their location and correction factors. Moreover, the local time of each station is used in the analysis to screen the observation times, and remove readings with a local time outside 0600 and 1300. With the observations of the different stations homogenized the fit provides now daily values of the hemispheric area at 1200 UT for all days within a region. The corresponding values of the latitude and CMT within the region are determined by linear interpolation to 1200 UT of each day covered by the region. Thus, a set of daily values of the averaged hemispheric areas together with their position are available. These can now be transformed into disk areas based on the distance μ from the center of the disk, which needs besides the latitude and CMT of the spot group also the latitude and longitude of the center of the disk from the physical coordinates of the Sun of that day. The sum of these daily values are then used to compare with the data from Balmaceda *et al.* (2009), the result of which is shown in Figs. 4a and 4b. The most important result is that the ratio of all data from the USAF/NOAA network and SOON is the same, which indicates that also the data from 1977–1981 need the same
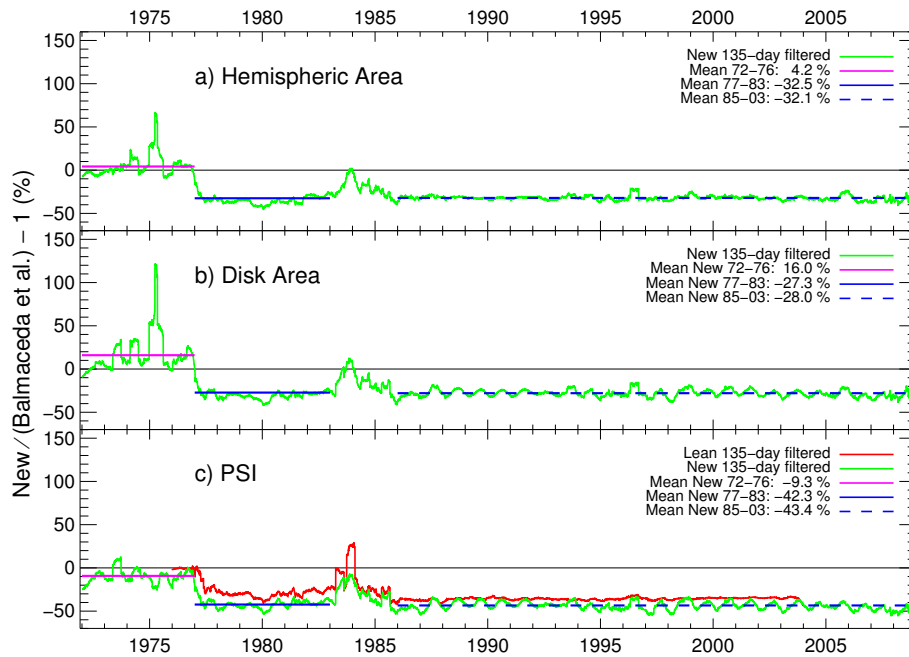
Figure 4. Comparison of the hemispheric (a), disk area (b) and PSI (c) time series as determined by Balmaceda *et al.* (2009) and those of the present analysis. The panel c) includes also the PSI used in Fröhlich & Lean (2004). The ratio for the period 1977–1981 and 1985–2003 are almost identical, which demonstrates the homogeneity of the full data set from the USAF/NOAA network.

correction. There is a major difference during three years around 1985 which may be due to a difference of the minimum sizes reported in the Russian and SOON records which is obviously most visible during minima. As similar differences are observed during the minimum of 1975 it may also be a problem of the way averages are determined.

The factor to be applied to the SOON data to make them compatible with the RGO data set can be determined from a direct comparison of the individual data points. This is illustrated in Fig. 5 as a scatter plot for the disk area comparison, similar ones have been produced for the hemispheric area and PSI. The results are summarized in Tab. 3 and the relations are determined with a linear fit to binned data points assuming the fitted line has to go through zero. For further calculations we will use the result of the disk area of 1.38 ± 0.05, which is close to the value of Balmaceda *et al.* (2009) of 1.43 ± 0.16, but determined without bridging the time between 1977 and 1985 with the Russian data. Moreover, it is, within the uncertainties, identical to the value of 1.4 determined earlier by Hathaway *et al.* (2002).
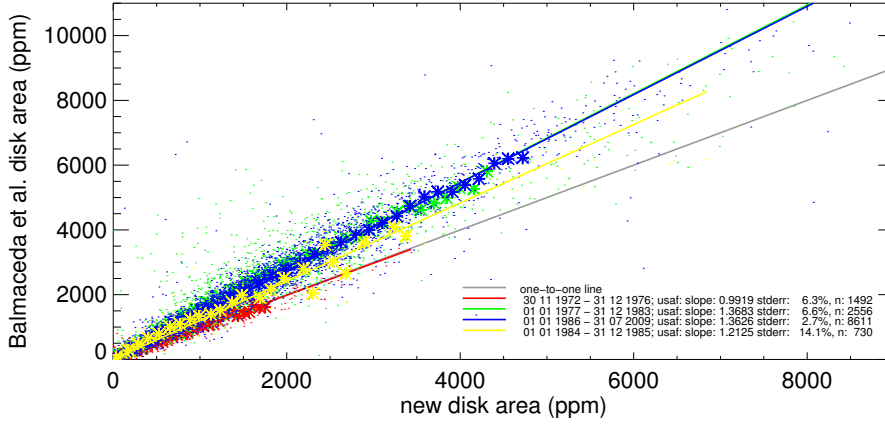
Figure 5. Direct comparison of the disk area from the present analysis and from Balmaceda *et al.* (2009). The different colors are for the different periods, the dots show all points and the asterisk 30 binned values from the range $0 \ldots \max/2$ of the new disk area.

Table 3. Summary of the results of the comparison of the new and Balmaceda *et al.* (2009) results for the different periods and averages as difference between the mean for the two periods after 1977 and the RGO value 1972–1976. The average result for the disk area is used in the following analysis to refer the SOON to the RGO, because this is the directly observed area.

	1972-1976	1977-1983	1986-2009	Average
Hemispheric	1.0369	1.5164	1.4777	1.444 ± 0.058
Disk	0.9919	1.3683	1.3626	1.377 ± 0.051
PSI	1.1259	1.4771	1.5731	1.355 ± 0.105

For the determination of PSI according to equation (2) we need, besides this correction, the contrast α_s. With typical values of the temperatures of the umbra and penumbra and their ratio, a value of 0.32 was first proposed by Hudson *et al.* (1982). From detailed observations of sunspots with the Vacuum Tower Telescope (VTT) of the Kiepenheuer Institute in Tenerife Steinegger *et al.* (1990) proposed a size dependent contrast according to

$$\alpha_s = (0.223 \pm 0.010) + (0.024 \pm 0.005) \log A_s \,. \tag{3}$$

Equation (3) was widely adopted (see *e.g.*, Brandt *et al.*, 1994; Fröhlich *et al.*, 1994; Fröhlich & Lean, 2004; Balmaceda *et al.*, 2009). Somewhat later Steinegger *et al.* (1996) deduced a refined size dependent contrast as

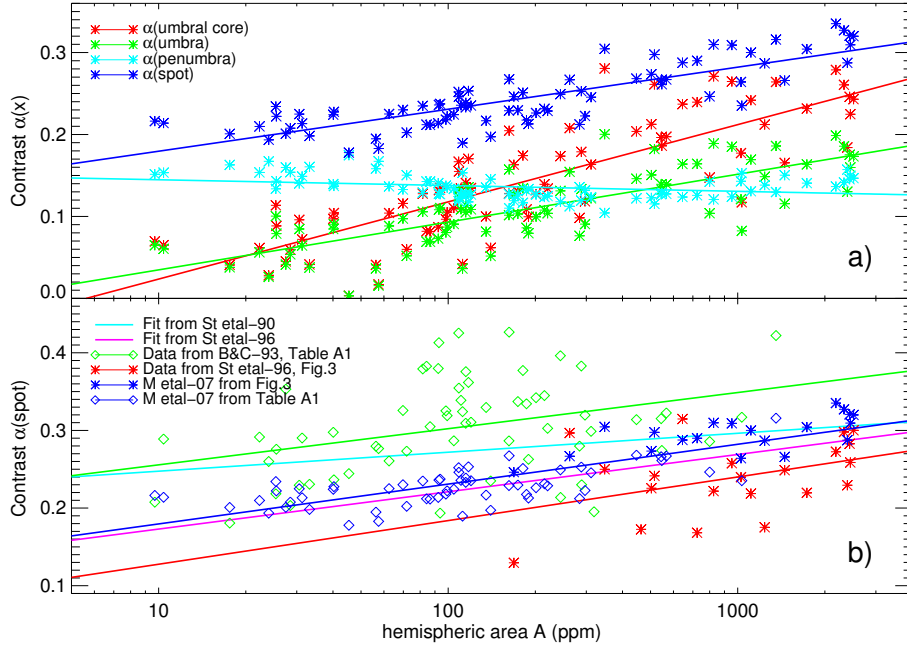$$\alpha_s = (0.125 \pm 0.019) + (0.048 \pm 0.010) \log A_s \,, \tag{4}$$

Figure 6. a) Contrast for umbral core C_{uc}, umbra C_u, penumbra C_p and spot $C_s = C_u + C_p$ calculated with intensities from the double linear fits of Tab. 2 of Mathew *et al.* (2007). b) Comparison with former contrast functions and the new C_s. The slopes of the different results are 0.047 ± 0.016, 0.056 ± 0.029, 0.051 ± 0.003, and 0.048 ± 0.010 for the original data of Beck & Chapman (1993), from the data of Fig. 3 Steinegger *et al.* (1996), from the data of Fig. 3 and Tab. A1 evaluated with the double linear fits of Mathew *et al.* (2007), and as published in Steinegger *et al.* (1996), respectively.

which showed a stronger size dependence, similar to the results from the San Fernando Observatory by Beck & Chapman (1993). More recently Mathew *et al.* (2007) presented results from sunspots observed by MDI/SOHO and determined size dependence of the contrast of the umbra and penumbra which can be compared to the findings of Steinegger *et al.* (1990, 1996), and Beck & Chapman (1993). Tab. A1 of Beck & Chapman (1993) provide data from 63 regions during the period from July 1985 to October 1990 and Fig. 3 of Steinegger *et al.* (1996) was digitized and provides another 22 observations of the NOAA regions 5521 and 5528 in June 1989. From these 85 observations some 45 are selected which have counterparts (same region on same day) in the SOON data set. The comparison of the areas of the San Fernando (telescopic) and the SOON areas amounts to $R = 1.25 \pm 0.25$ for all results with $0.8 < R < 1.5$ and

Table 4. Listed are center-to-limb function coefficients $a_{0.2}$ used in the calculation of the different PSI values with the indices of the last column. $C_\lambda/C_{\mathrm{tot}}$ provides the factor used to scale the contrast for the different wavelengths.

Wavelength	a_0	a_1	a_2	$C_\lambda/C_{\mathrm{tot}}$	Index
total Eddington	0.4000	0.6000	0.0000	1.000	0
total Pierce	0.3600	0.8400	−0.2000	1.000	1
335 nm Pierce	0.1073	0.9465	−0.0538	0.733	2
402 nm Pierce	0.1412	0.9103	−0.0515	0.801	3
500 nm Pierce	0.2500	0.9700	−0.2200	0.885	4
677 nm Pierce	0.4153	0.8128	−0.2280	1.000	5
862 nm Pierce	0.5192	0.6957	−0.2149	1.079	6

$R = 1.38 \pm 0.53$ for the observations of Tenerife. Both indicate a similar ratio as the analysis above. So, it may indeed be due to the difference between the determination of the area from drawings and images. Fig. 6 shows the result of the comparison with a) the different contrast for the spot data from Tenerife and San Fernando using the double linear fits of Tab. 2 of Mathew *et al.* (2007) and b) the comparison of the different determinations. The coefficients of equation (4) may be adapted to the weighted average of the original and new determination, using 0.13 ± 0.02 and 0.05 ± 0.01. The contrast depends also on wavelength and with the size dependence kept constant this can be taken into account with the contrast ratio $C_\lambda/C_{\mathrm{tot}}$ from Tab. 4 to scale α for different wavelengths.

As in the former version of my program I use different center-to-limb variations, the standard Eddington limb darkening $R(\mu) = (3\mu + 2)/5$ or more elaborate functions of μ from Livingston (2000, Tab. 14.17) for modeling total or also spectral solar irradiance variations at the following wavelengths 335, 402, 500, 677, and 862 nm. The center-to-limb variation is described by three coefficients according to $R(\mu) = a_0 + a_1\mu + a_2\mu^2$ which obviously can also be used for the Eddington function. The coefficients $a_{0.2}$ for the different wavelengths are listed in Tab. 4 together with the wavelength dependence of the contrast, which is determined from Livingston (2000, Tab. 14.17) with $A_u/A_p = 0.248$ from Beck & Chapman (1993) and relative to the MDI wavelength, which then has a value of unity.

Finally the result of the PSI evaluation is provided in a daily data set with 26 columns: date, disk area (ppm of the disk), hemispheric area (μhem or ppm of the hemisphere), $P_S(0:6)$ (in ppm and index as of Tab. 4, last column) and $P_S(1)$ values separated into 16 latitude bins from $-0.8 \le \sin(\mathrm{lat}) \le +0.8$. As an example the latter data are plotted as a butterfly diagram in Fig. 7 from 1972 to present. Note the important difference of the minimum 2008 to those before, with essentially no overlap of cycle 23 and and the upcoming 24.
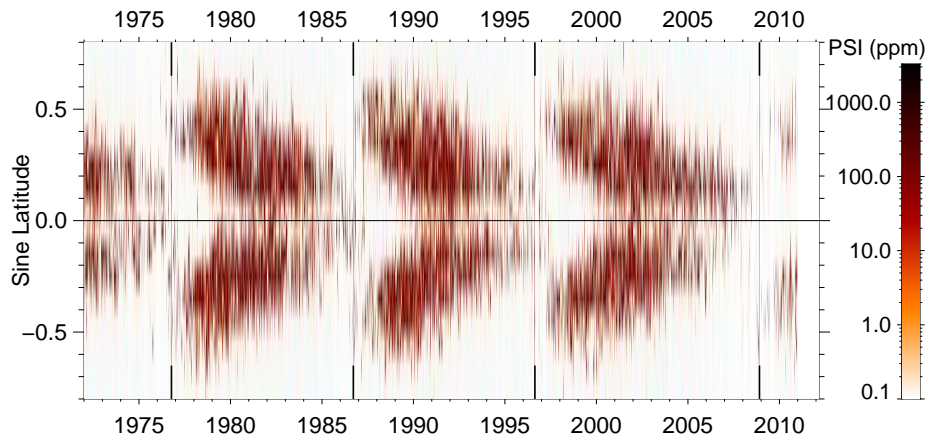
Figure 7. Daily values of PSI as a function of the latitude providing the famous butterfly diagram of sunspots. At the beginning of a cycle they start at latitudes around $\pm 40^\circ$ and then migrate down towards the equator. The vertical lines indicate the time of the minima and it becomes also clear that they are determined by the first important sunspots emerging at high latitudes. Note that before 1977 the RGO data are used and afterwards those from the USAF/SOON network.

3.2. Influence of faculae and network

Images of the Sun, called spectroheliograms, which are observed in a narrow wavelength band in the resonance line of, *e.g.*, Ca II K at 393.37 nm, the strongest solar spectral line observable from the ground, can provide areas covered by plages and a bright network in the upper solar atmosphere, the chromosphere. These can be used to determine the effect of photospheric faculae and the network on TSI. At Kitt-Peak Observatory monthly observations of disk-integrated Ca II K-line fluxes started in 1975 and proved to be a good surrogate for the plage and network area deduced from images (see Fig. 2c). With the start of the NOAA mission NIMBUS7 observations of the core-to-wing ratio of the Mg II H & K lines, called Mg II index (Heath & Schlesinger, 1986), became available. There has been a continuous daily record since November 1978 (Viereck *et al.*, 2010), which is weekly updated with SOLSTICE/SORCE data and widely used as a surrogate for the facular and network influence. As explained in Fröhlich & Lean (2004), Domingo *et al.* (2009), and Fröhlich (2009b) the time series of the Mg II index, shown in Fig. 2d, is separated into a short- and long-term part, Mg II-st and Mg II-lt, which is performed by calculating a running average of the standard deviation over 217 days (8 solar rotations) which is then used - multiplied by an appropriate factor - to define the lower limit of the short-term variations of the Mg II index. The values above this limit form the short-term part of Fig. 8b and the values below the long-term part of Fig. 8c. The reason for
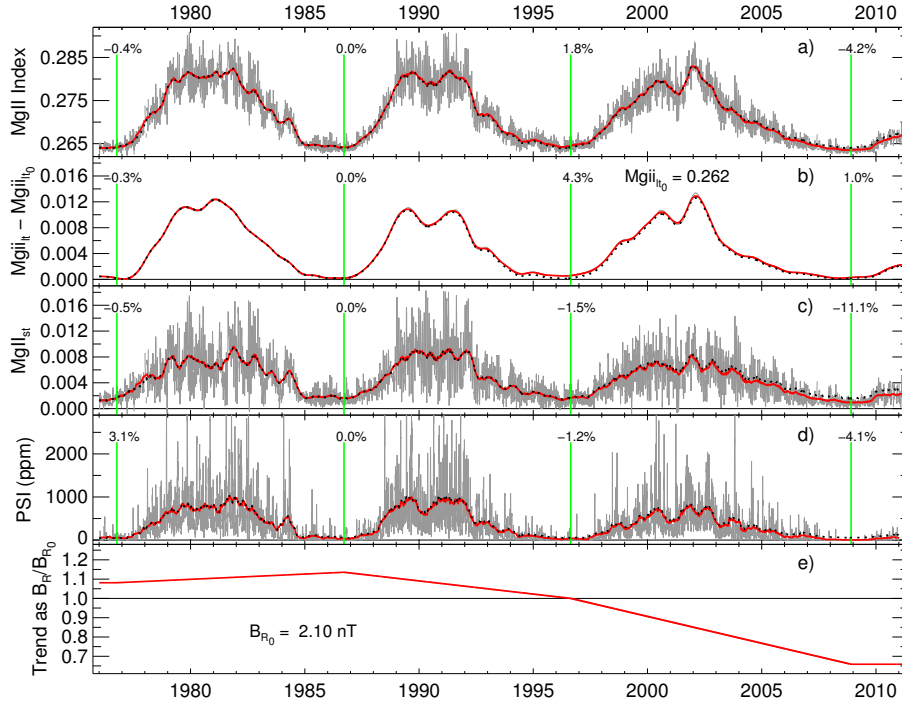
Figure 8. a) shows daily values of the Mg II index as observed and decomposed into b) a long- (Mg II-lt) and c) a short-term (Mg II-st) part. d) is the PSI from Section 3.1. Times of the minima are given as vertical green lines and are labeled with the percentage deviation of that minimum from the value of the minimum around 1986 relative to the mean amplitude of the parameter. The dotted lines correspond to the parameter if the linear trend between minima is removed. e) shows the trend of B_R from Section 2 as a ratio daily values relative to the value during 1996 minimum.

calling the short-term part the facular contribution is quite clear - it is related to the passage of active regions on the rotational timescale. As shown below, the long-term part gets a different coefficient from the multi-linear regression analysis which confirms the usefulness of separating the two. So the daily Mg II-lt values are used for $P_N(t)$ and those of Mg II-st for $P_F(t)$ in equation (1), providing the second and third component of the proxy model. Figure 8c and 8d illustrate the influence of faculae and network during the recent minimum. The lower value of the Mg II index during the recent minimum is mainly determined by the smaller number of faculae and not by the solar cycle modulation part.

3.3. Influence of the intra-cycle trend

The intra-cycle trend used in the proxy model is shown in Fig. 8e. It is presented as the ratio of B_R/B_{R_0} with B_{R_0} being the value during the minimum 1996. The

B_R at minima are determined as an average over 217 days (8 solar rotations) centered at the minimum date and amount to 2.27, 2.38, 2.10, and 1.38 nT for the last four minima. Between the minima the trend is linearly interpolated and for the time before the minimum 1975 and after 2008 the slope is assumed to be zero.

4. Calibration of the four-component model and discussion of the results

The value of the quiet Sun, S_Q, and the coefficients $a_{F,N,S,T}$ are determined by a multi-linear regression according to equation (1) with the new $p_S S_Q 10^{-6}$ and the $P_{F,N,T}$ against the extended PMOD composite for $S(t)$. The results are shown in Tab. 5 and Fig. 9.

Table 5. Coefficients of the 4-component model. S_Q is in Wm^{-2}, the others in Wm^{-2} per Mg II units, ppm and nT, respectively. The standard errors for the coefficients are given as 1-σ values in the units of the coefficients and in percent.

S_Q	a_F	a_N	$\frac{a_S}{S_Q}$	$\frac{a_T}{B_{R_0}}$	r^2
1364.70 ± 0.02	76.20	122.93	-0.8102	0.331	0.8470
standard error 1-σ	1.00	0.72	0.0048	0.006	
standard error (%)	1.3	0.6	0.6	1.9	

Earlier results of the three-component model (*e.g.*, Fröhlich & Lean, 2004) showed that 78.6 % of the variance are explained. The four-component model shown here increases the variance explained to 84.7 %, which is an important improvement. The use of equation (4) (with modified coefficients) instead of equation (3) for the contrast of spots does improve the correlation only slightly, but changes the coefficients significantly (Fröhlich, 2011b). Another interesting result is that a linear fit to the difference between observed and model TSI over 36 years has a slope of only 7.2 ± 0.2 mWm^{-2}/decade or about 5 ppm/decade which is compared to the downward trend during cycle 23 of about 200 ppm/decade negligible and demonstrates the importance of including the trend according to the TSI–B_R correlation. The difference in value of the long- and short-term Mg II index is known for some time and Fröhlich & Lean (2004) suggested that this difference is due to the increasing specific contrast from faculae to network as shown by Ortiz *et al.* (2006). The application of the 3-component model to Ly-α and EUV from SOHO/SEM shows, however, a similar difference which means that the specific contrast cannot be the reason, mainly because this effect is limited to radiation emitted from the photosphere. The difference in area coverage of the two parts may explain the difference. The short-term part is limited to the active regions in a limited latitude band whereas the long-term is
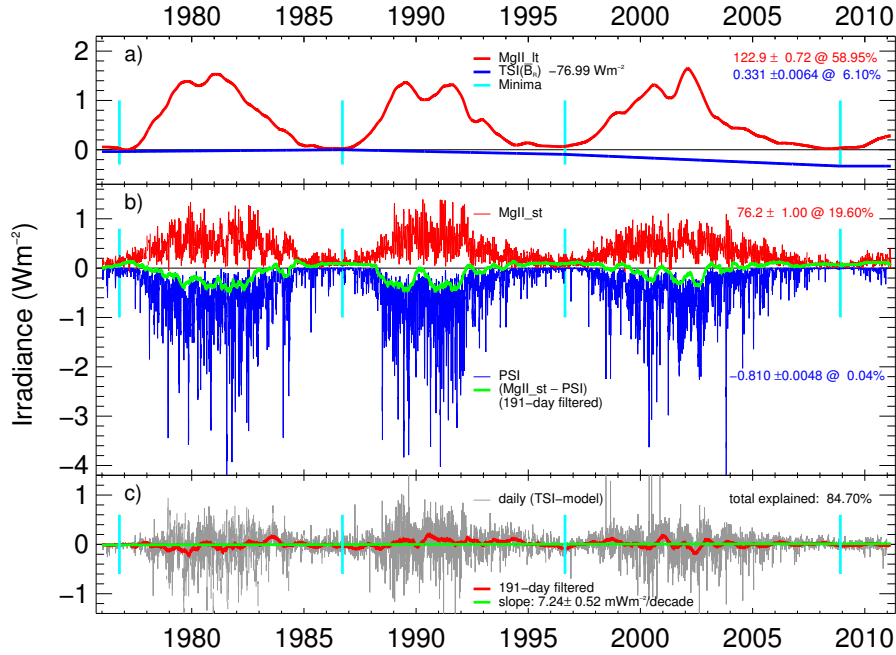
Figure 9. a) shows the calibrated long-term (Mg II-lt (red) together with the corresponding trend (blue) of the 'quiet sun', and b) the calibrated short-term (Mg II-st (red) and PSI (blue). Note that all three panels have the same scale. The green curve of b) shows the 191-day filtered difference between facular and sunspot influence. The net effect of active regions increases TSI during minima by $\approx 0.08\,\mathrm{Wm^{-2}}$, whereas during maxima TSI is dominated by sunspots and a decrease by $\approx 0.25\,\mathrm{Wm^{-2}}$ is observed. c) shows the daily difference between and TSI and the model.

all over the disk. A simple calculation provides an area ratio of 1.5 with a latitude range of ± 22 degree for the short-term part which is a reasonable average of the activity band over a solar cycle.

The trend is well represented in the model with a slope of the TSI–B_{R} relation of 0.331 ± 0.006 which is close to the result of the direct correlation of 0.35 ± 0.14 shown in Fig. 3c. The somewhat smaller value from the model indicates that some of the trend is due to less magnetic elements, *e.g.*, faculae during the recent minimum. The difference is about 6 %, which is compatible with the average change over cycle 23 of the order of 6 % for SSN, F 10.7 and the chromospheric indices (Tab. 1). This confirms the need for the fourth component of the TSI proxy model to account for the trend which is related to the strength of the activity; the details, however, of its origin are not yet understood. As suggested by Tapping *et al.* (2007) and Fröhlich (2009a) an obvious mechanism

would be a small global temperature change of the Sun of about 0.25 K, which would explain the different long-term behavior of TSI and UV–EUV irradiance. Recently Foukal *et al.* (2011) suggested that the effect of the increase of the contrast of magnetic elements with decreasing field as found by, *e.g.*, Ortiz *et al.* (2006) from the analysis of MDI data, may be the mechanism for the stronger trend in TSI than for chromospheric radiation, because this effect is only relevant to the photosphere. So, during the last minimum the chromospheric temperature distribution was determined by the low flux density of the remaining magnetic elements, whereas the effect on TSI is amplified by a factor of four by the increased contrast of the same magnetic elements. Such an effect is not included in the SATIRE model which may explain why it is unable to reproduce the observed trend in TSI (Krivova *et al.*, 2011).

5. Conclusions

The results of this analysis show clearly the need for a trend independent of the direct influence of spots, faculae and network. On the other hand the intra-cycle variation is well described by the three-component model alone. Independent of the explanation of this effect it means that the UV radiation originating from the chromosphere has a much smaller – at least by a factor of 4-5 – long-term trend than TSI. The results of the present analysis indicate that about 20 % of the trend in TSI is attributed to the direct influence of the manifestations of surface magnetism, the rest is possibly due to the influence of the increasing contrast of flux tubes with decreasing area which is relevant to the photosphere and is not influencing the chromosphere.

References

Ball, W. T., Unruh, Y. C., Krivova, N. A., Solanki, S., Harder, J. W.: 2011, *Astron. Astrophys.* **530**, A71

Balmaceda, L.A., Solanki, S.K., Krivova, N.A., Foster, S.: 2009, *J. Geophys. Res.* **114**, A07104

Beck, J.G., Chapman, G.A.: 1993, *Sol. Phys.* **146**, 49

Brandt, P.N., Stix, M., Weinhardt, H.: 1994, *Sol. Phys.* **152**, 119

Charbonneau, P.: 2005, *Living Reviews in Solar Physics* **2**, 2, available at `http://solarphysics.livingreviews.org/Articles/lrsp-2010-3/`

Domingo, V., Ermolli, I., Fox, P., Fröhlich, C., Haberreiter, M., Krivova, N., Kopp, G., Schmutz, W., Solanki, S.K., Spruit, H.C., Unruh, Y., Vögler, A.: 2009, *Space Sci. Rev.* **145**, 337

Eddy, J.A.: 1976, *Science* **192**, 1189

Foukal, P., Ortiz, A., Schnerr, R.: 2011, *Astrophys. J., Lett.* **733**, L38

Fröhlich, C.: 2006, *Space Sci. Rev.* **125**, 53

Fröhlich, C.: 2009a, *Astron. Astrophys.* **501**, L27

Fröhlich, C.: 2009b, in *Selected Papers from the 2007 Kyoto Symposium: Climate and Weather of the Sun-Earth System (CAWSES)*, eds.: T. Tsuda, R. Fujii, K. Shibata, and M.A. Geller, Terra Publishing, available at `http://www.terrapub.co.jp/onlineproceedings/ste/CAWSES2007/index.html`, Tokyo, 217

Fröhlich, C.: 2011a, in *Encyclopedia of Sustainability Science and Technology*, ed.: Robert A. Meyers, Springer Science-Business Media, LLC, New York, Article 443, in press

Fröhlich, C.: 2011b, *Space Sci. Rev.* **158**, published online 11 May 2011

Fröhlich, C., Lean, J.: 2004, *Astron. Astrophys. Rev.* **12**, 273

Fröhlich, C., Pap, J.M., Hudson, H.S.: 1994, *Sol. Phys.* **152**, 111

Hagenaar, H.J., De Rosa, M.L., Schrijver, C.J.: 2008, *Astrophys. J.* **678**, 541

Harvey, K.: 2000, in *Encyclopedia of Astronomy and Astrophysics*, ed.: P. Murdin, Institute of Physics Publishing, Bristol, U.K., Article 2275

Hathaway, D.H., Wilson, R.M., Reichmann, E.J.: 2002, *Sol. Phys.* **211**, 357

Heath, D.F., Schlesinger, B.M.: 1986, *J. Geophys. Res.* **91**, 8672

Hoyt, D.V., Eddy, J.A.: 1982, *An Atlas of Variations in the Solar Constant Caused by Sunspot Blocking and Facular Emissions from 1874 to 1981*, NCAR Technical Note NCAR/TN-194+STR, NCAR Boulder, CO USA

Hoyt, D.V., Eddy, J.A., Hudson, H.S.: 1983, *Astrophys. J.* **275**, 878

Hudson, H.S., Silva, S., Woodard, M., Willson, R.C.: 1982, *Sol. Phys.* **76**, 211

Hudson, H.S., Willson, R.C.: 1981, *Adv. Space Res.* **1(13)**, 285

Krivova, N. A., Solanki, S. K., Fligge, M., Unruh, Y. C.: 2003, *Astron. Astrophys.* **399**, L1

Krivova, N. A., Solanki, S. K., Schmutz, W.: 2011, *Astron. Astrophys.* **529**, A81

Livingston, W.C.: 2000, in *Allen's Astrophysical Quantities*, ed.: Arthur N. Cox, Springer Verlag, New York, 339

Lockwood, M., Fröhlich, C.: 2008, *Proc. R. Soc. A* **464**, 1367

Mathew, S.K., Martínez Pillet, V., Solanki, S.K., Krivova, N.A.: 2007, *Astron. Astrophys.* **465**, 291

Ortiz, A., Domingo, V., Sanahuja, B.: 2006, *Astron. Astrophys.* **452**, 311

Pap, J.: 1993, Differences between sunspot data, earlier available (*e.g.*, used by Hugh Hudson) and presently published in SGD tables at NGDC, private comm.

Steinegger, M., Brandt, P.N., Pap, J., Schmidt, W.: 1990, *Astrophys. Space Sci.* **170**, 127

Steinegger, M., Vazquez, M., Bonet, J.A., Brandt, P.N.: 1996, *Astrophys. J.* **461**, 478

Steinhilber, F.: 2010, *Astron. Astrophys.* **523**, A39

Steinhilber, F., Beer, J., Fröhlich, C.: 2009, *Geophys. Res. Lett.* **36**, L19704

Tapping, K.F., Boteler, D., Charbonneau, P., Crouch, A., Manson, A., Paquette, H.: 2007, *Sol. Phys.* **246**, 309

Viereck, R.A., Snow, M., Deland, M.T., Weber, M., Puga, L., Bouwer, D.: 2010, *AGU Fall Meeting Abstracts* **B877**,

Wenzler, T., Solanki, S. K., Krivova, N. A.: 2009, *Geophys. Res. Lett.* **36**, L11102

Wenzler, T., Solanki, S. K., Krivova, N. A., Fröhlich, C.: 2006, *Astron. Astrophys.* **460**, 583